Arch. Metall. Mater. **64** (2019), 3, 863-867

DOI: 10.24425/amm.2019.129462

SEUNG-JIN OH*, BYOUNG-CHEOL KIM**, MAN-CHUL SUH**, IN-JIN SHON*, SEOK-JAE LEE*#

INFLUENCE OF CARBON CONTENT ON AUSTENITE STABILITY AND STRAIN-INDUCED TRANSFORMATION OF NANOCRYSTALLINE FeNiC ALLOY BY SPARK PLASMA SINTERING

The effects of carbon content on the austenite stability and strain-induced transformation of nanocrystalline Fe-11% Ni alloys were investigated using X-ray analysis and mechanical tests. The nanocrystalline FeNiC alloy samples were rapidly fabricated using spark plasma sintering because of the extremely short densification time, which not only helped attain the theoretical density value but also prevented grain growth. The increased austenite stability resulted from nanosized crystallites in the sintered alloys. Increasing compressive deformation increased the volume fraction of strain-induced martensite from austenite decomposition. The kinetics of the strain-induced martensite formation were evaluated using an empirical equation considering the austenite stability factor. As the carbon content increased, the austenite stability was enhanced, contributing to not only a higher volume fraction of austenite after sintering, but also to the suppression of its strain-induced martensite transformation.

Keywords: FeNiC alloy, austenite stability, strain-induced transformation, spark plasma sintering

1. Introduction

In recent years, studies on multiphase steels such as medium Mn TRIP steels and Q&P steels have been conducted to improve the strength of steel based on metastable retained austenite at room temperature [1,2]. The alloys can improve both ductility and tensile strength based on strain-induced martensite transformation from austenite when plastic deformation occurs [3]. Therefore, controlling the stability and fraction of austenite at room temperature is the most important factor for improving the mechanical properties of Fe-based alloys. The austenite stability should be increased so as to retain some amount of austenite at room temperature. Austenite stability can be enhanced by controlling the chemical composition [4,5]. The austenite stability is enhanced when increasing the amount of austenite-stabilizing elements such as Ni, Mn, and C. Carbon is known to be the most effective element for increasing the austenite stability. The austenite stability is also influenced by grain size. Grain refinement is also very effective for increasing austenite stability. Lee et al. [6] reported that a high austenite fraction was obtained by reducing the grain size to 300 nm in ultra-fine-grained TRIP steel containing 6 wt.% Mn. Matsuika et al. [7] reported that the thermal stability of austenite increases as the grain size decreases in metastable austenitic stainless steels.

Powder metallurgy is a manufacturing process that can overcome the limitations of grain refinement in the conventional process. Mechanical alloying (MA), a technique in powder metallurgy, is a relatively simple and effective process, as compared to conventional alloying. Mechanical alloying involves a repetition of two processes, cold welding and fracturing between powders, in which the powders of metals, ceramics, and mixtures can be alloyed using a high-energy ball mill [8]. Ball-milling is a very efficient process for producing powders with nanosized crystallites and minimizing the diffusion distance of the atoms to facilitate alloying. Among the various sintering methods, in spark plasma sintering (SPS, pressure and a pulse current are directly applied to a mold containing powder to sinter the sample in a short time. Thus, various studies applying SPS to nanocrystalline structures, porous materials, ceramic materials, and iron-based materials have been reported [9-12]. Fe-Ni alloys are used in various materials such as stainless steel, invar, and maraging steel because of their special magnetic, thermal, and mechanical properties [13,14]. Some research into Fe-Ni alloys through MA and SPS has been conducted [15]. However, there are few studies on the austenite stability and strain-induced transformation considering the carbon effect in Fe-Ni alloys produced by MA and SPS.

Therefore, in this study, FeNiC alloy powders were prepared using a high-energy ball mill, and nanocrystalline FeNiC alloys were prepared using SPS. Especially we changed the carbon content that is known as a very strong austenite stabilizing element. Other variables such as milling and sintering conditions were controlled identically. The crystallite size of the alloy powders and phase fraction of the sintered alloys were measured quan-

* CHONBUK NATIONAL UNIVERSITY, DIVISION OF ADVANCED MATERIALS ENGINEERING, 567 BAEKJE-DAERO, DEOKJIN-GU, JEONJU, 54896, REPUBLIC OF KOREA
** KOREA POLYTECHNIC UNIVERSITY, SIHEUNG, REPUBLIC OF KOREA
# Corresponding author: seokjaelee@jbnu.ac.kr

titatively and the behavior of strain-induced martensite under plastic deformation was analyzed.

2. Experimental Procedure

Nanocrystalline Fe-11 wt.% Ni-*x* wt% C (*x* = 0, 0.2, 0.5) alloy powder was prepared using a high-energy ball mill. Fe powder (MKT Corp., Korea) of 99.9% purity and an average particle size of <23.9 μm, Ni powder (Alfa Aesar, Korea) of 99.9% purity and an average particle size of <7 μm, and graphite powder (Alfa Aesar, Korea) of 99% purity and a typical particle size of 7-11 μm were used. Stearic acid [$CH_3(CH_2)_{16}CO_2H$, Alfa Aesar, Korea] was used as the process control agent. Mechanical alloying was carried out at 250 rpm for 24 h in an Ar atmosphere using a high-energy ball mill (Fritsch, Pulverisette-5, oil milling) and the ball-to-powder ratio (BPR) was set at 30:1. A tungsten carbide ball of diameter 9 mm and a stainless container were used. The balance between cold welding and fracturing was controlled by adding 1 wt.% of process control agent. The milled alloy powder was poured into a cylindrical graphite mold with an outer diameter of 35 mm, an inner diameter of 10 mm, and a height of 40 mm, followed by sintering using SPS. Sintering was carried out at 1,000°C/min, to 1,000°C, under a high vacuum of 150 mTorr or less and uniaxial pressure of 80 MPa, which was immediately followed by cooling to room temperature. The relative density of the sintered alloy was measured using the Archimedes method. Powder analysis was performed using X-ray diffraction (XRD, RIGAKU Max-2500). A Cu Kα target was used; measurements were made at 40 kV and 100 mA. The structural properties of the powder including grain size and lattice strain were analyzed using the Williams and Hall equation. Cylindrical samples of height 4 mm and diameter 4 mm were prepared from the sintered alloys for use in compressive tests. The compressive tests were conducted at a speed of 1×10^{-3} s^{-1} using a universal testing machine (Instron 8801). The austenite phase fraction during the compressive test was determined by calculation using the diffraction peak intensity from the X-ray diffraction measurement.

3. Results and discussion

Figure 1 shows the XRD results for the FeNiC alloy powder prepared using MA with a high-energy ball mill. Only a single α-Fe peak was detected in the alloy powders. The equilibrium solubility of Ni in Fe is reported to be 3.5 wt.% [16], but MA can increase the Ni solubility in Fe to 30 at.% [17]. The crystallite size and lattice strain of the powder can be calculated using the Williams and Hall equation using the full width at half maximum (FWHM) and Bragg angles at the XRD peak [18].

$$B_r \cos\theta = \frac{k \cdot \lambda}{D} + \eta \sin\theta \qquad (1)$$

where B_r is the FWHM of the milled powder's XRD peak, θ is the Bragg angle, λ is the wavelength of the Cu Kα target, D is the crystallite size, η is the lattice strain, k is a constant. The crystallite size and lattice strain of the alloy powders were 11-16 nm and 0.2-0.3%, respectively. The effect of carbon on the crystallite size was assumed to be negligible.

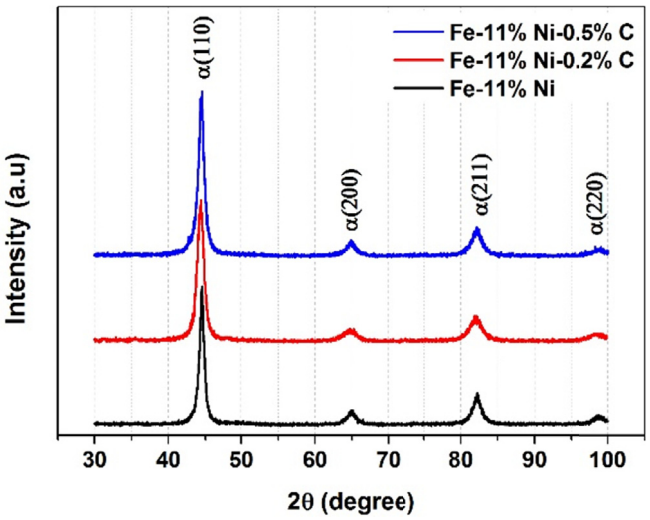

Fig. 1. XRD patterns of the milled Fe-11 wt.% Ni- *x* wt.% C (*x* = 0, 0.2, 0.5) powders

Table 1 shows the relative densities obtained from measured densities and theoretical densities, calculated using the mixing ratio of the sintered alloys [19]. Each sample was well-densified during SPS and had a density similar to the theoretical density. The relative density increased as the carbon content increased.

TABLE 1

Densities of sintered alloys with different carbon content

Density	Fe-11%Ni	Fe-11%Ni-0.2%C	Fe-11%Ni-0.5%C
Theoretical (g/cm^3, A)	7.972	7.944	7.833
Measured (g/cm^3, B)	7.721	7.722	7.793
Relative (%, = B/A×100)	97.0%	97.2%	99.5%

Figure 2 shows the XRD peaks of the sintered FeNiC alloys. As the carbon content is increased from 0 to 0.5 wt.%, the intensities of the γ(200), γ(220), γ(311) austenite peaks gradually increased. The measured volume fractions of austenite from the XRD peaks in the Fe-11%Ni, Fe-11%Ni-0.2%C, and Fe-11%Ni-0.5%C samples were 64, 76, and 90 vol.%, respectively. Carbon is a representative austenite stabilizing element. The volume fraction of retained austenite was calculated from the XRD results using the Averbach and Cohen method [20]. Recently, it has been reported that the austenite volume fraction obtained by XRD analysis was well matched with that obtained by microstructural EBSD analysis in the sintered Fe-Mn alloys [12,21]. Thermodynamically, no austenite phase can exist at room temperature in pure Fe because the austenite phase is stable phase at high temperatures. The addition of certain alloying elements for stabilizing austenite can help retain the austenite

at room temperature. However, it is reported that no retained austenite exists at room temperature in bulk Fe-Ni alloys with a Ni content of 11 to 23 wt.% [22]. Recently, Park et al. [23] fabricated the nanocrystallinte Fe-(11-15)% Ni alloys by SPS and observed the initial volume fraction of austenite between 48 and 83 vol.%. Similarly, in this study, austenite of 64 vol.% was successfully obtained in Fe-11 wt.%Ni alloy by the addition of Ni as well as refinement of actual grain size. The crystallite size was several tens of nanometers when using MA with high-energy milling and SPS with a very short sintering time. As the crystallite size of the alloy powder decreases, the stability of the austenite increases and retained austenite can exist, even at room temperature. It is reported that the effect of grain refinement on the increases in the austenite stability is caused by suppressing the decomposition of austenite [24].

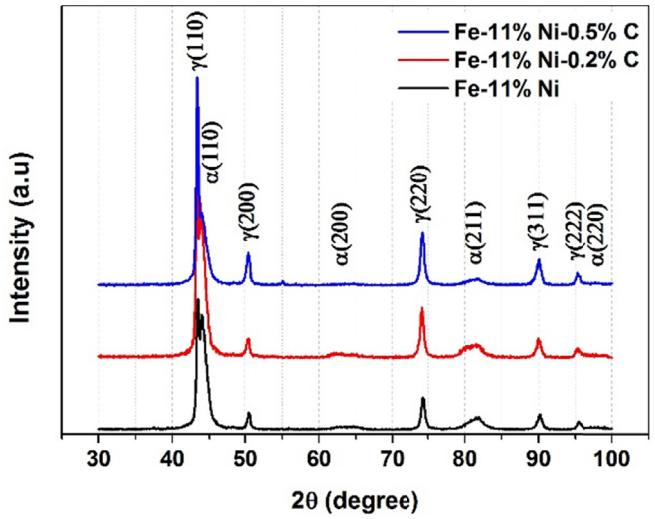

Fig. 2. XRD patterns of the sintered Fe-11 wt.% Ni-x wt.% C (x = 0, 0.2, 0.5) alloy

Figure 3 shows the compressive stress-strain curves of the sintered FeNiC samples. The yield strength is decreased as the carbon content is increased because of the larger volume fraction of austenite. Wang and coworkers reported that the yield strength decreased gradually with the decrease of initial fraction of martensite in quenching and partitioned steel consisting of martensite and retained austenite [25]. Figure 4 shows the XRD results of the sintered FeNiC samples after compressive deformation. As the compressive strain increases, the intensi-

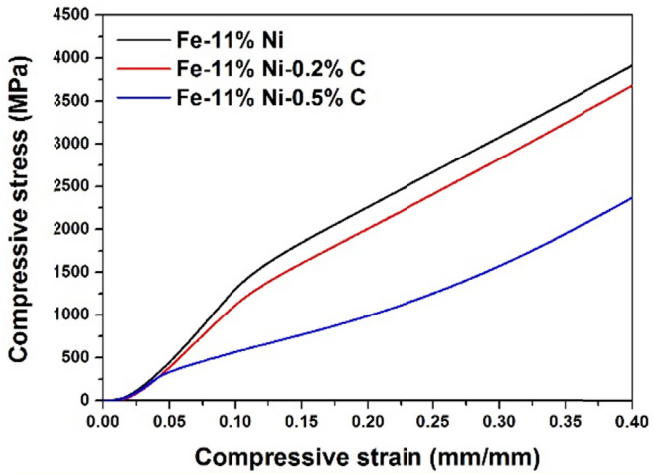

Fig. 3. Compressive stress-strain curves of the sintered Fe-11 wt.% Ni-x wt.% C (x = 0, 0.2, 0.5) alloy

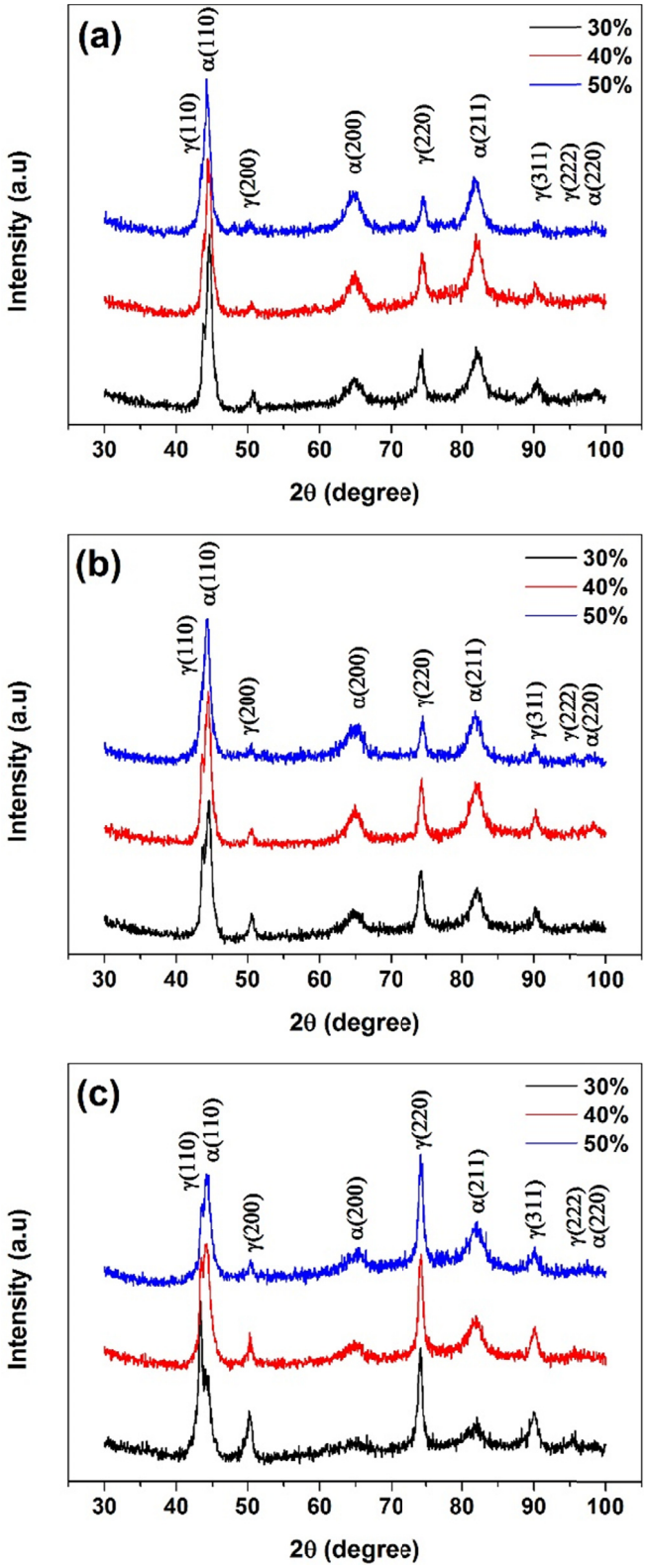

Fig. 4. XRD patterns of the sintered alloy after compressive test: (a) Fe-11%Ni (b) Fe-11%Ni-0.2%C, and (c) Fe-11%Ni-0.5%C

ties of the austenite peaks in all sintered alloys are gradually lowered (relatively). This implies that the metastable austenite transforms to strain-induced martensite as compressive strain increases. Figure 5 shows that the volume fraction of metastable retained austenite varied with the compressive strain. After 50% deformation, the volume fraction of the retained austenite in Fe-11%Ni, Fe-11%Ni-0.2%C, and Fe-11%Ni-0.5%C sintered alloys decreased to 40%, 54%, and 74%, respectively. The ratio of the fraction of the strain-induced martensite to the initial fraction of retained austenite(= $V_{\alpha'}/V_{\gamma}^{0}$) was calculated to be 0.375, 0.289, and 0.178 for Fe-11%Ni, Fe-11%Ni-0.2%C, and Fe-11%Ni-0.5%C alloys, respectively. This means that the austenite stability increased by adding carbon, resulting in suppression of the transformation kinetics of strain-induced martensite from austenite during plastic deformation.

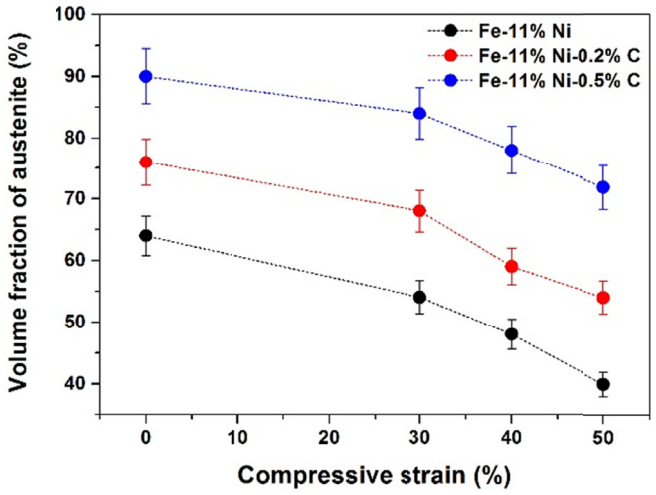

Fig. 5. Effect of carbon content on the variation of volume fraction of metastable austenite during compressive test

The kinetics model for strain-induced martensite formation was adopted to evaluate the effect of carbon addition on the austenite stability. Among several kinetics models, the BMT model proposed by Burke et al. [26], Matsumura et al. [27], and Tsuchida [28] was used to compare the behavior of the strain-induced martensite transformation in this study. The BMT model equation is as follows:

$$V_{\alpha'} = \frac{V_{\gamma}^{0}}{1 + p/(k\varepsilon^{p} V_{\gamma}^{0})} \qquad (2)$$

where $V_{\alpha'}$ is the fraction of the strain-induced martensite, V_{γ}^{0} is the fraction of initial austenite, and ε is the plastic strain. k is a constant related to austenite stability. p is a constant indicating the influence of the autocatalytic effect; when there is no autocatalytic effect, the p value is 1.0. As the grain size decreases, the nucleation rate of the martensite transformation accelerates. Thus, the p value was set to 2 in this study. Figure 6 compares the transformation behavior of the strain-induced martensite predicted using the BMT model with the measured values. The prediction results have very high accuracy. The k values related to the austenite stability were determined to be 6.984, 4.325, and 2.168 for Fe-11%Ni, Fe-11%Ni-0.2%C, and Fe-11%Ni-0.5%C sintered alloys, respectively. The k value tends to decrease gradually as the carbon content increases, implying that the austenite stability is increased. These results are consistent with the results of austenite volume fraction change for different

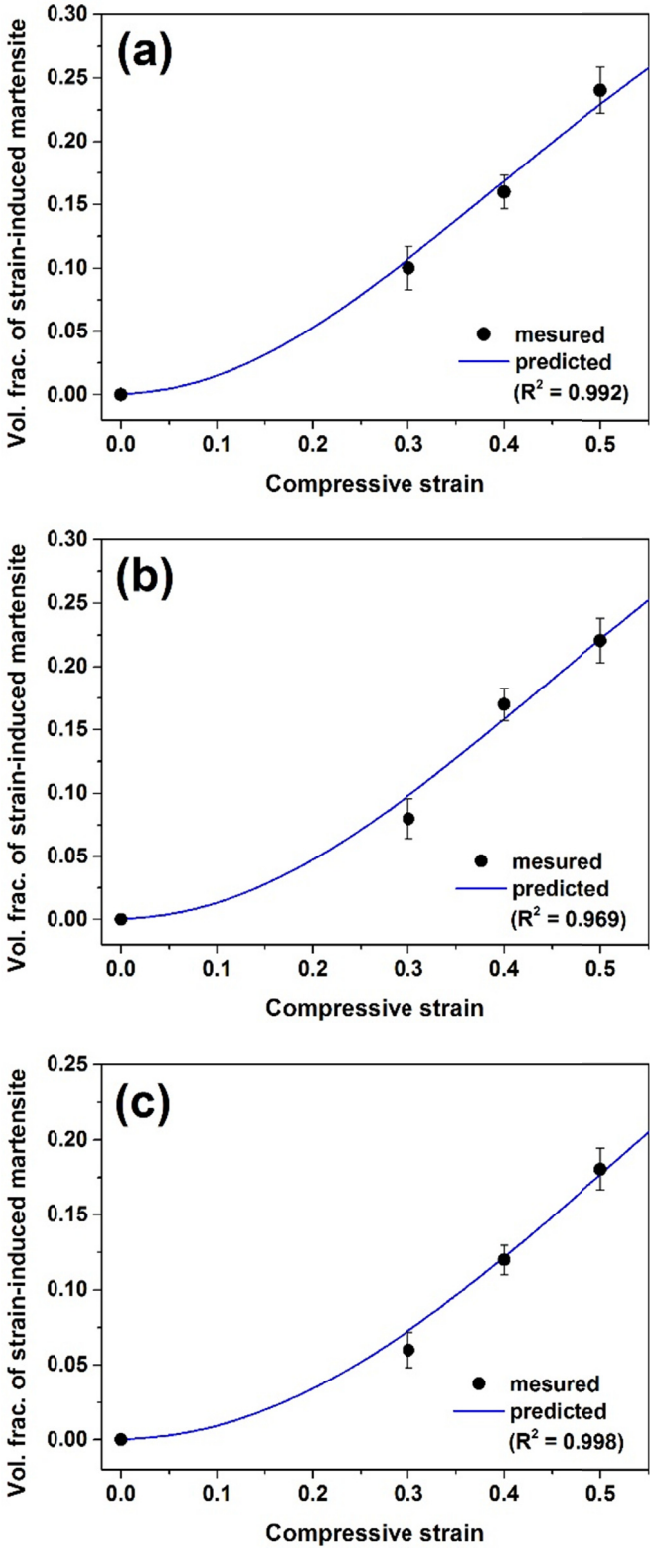

Fig. 6. Comparison of strain-induced martensite transformation kinetics depending on carbon content: (a) Fe-11%Ni (b) Fe-11%Ni-0.2%C, and (c) Fe-11%Ni-0.5%C

carbon contents. The increase in carbon content increases the austenite stability, resulting in both the higher volume fraction of austenite after the sintering and the retarded transformation kinetics during deformation.

4. Conclusions

In this study, nanocrystalline FeNiC alloy powders were prepared using a high-energy ball mill. Nanocrystalline FeNiC alloys were successfully fabricated using SPS. The crystallite size of the alloy powders was calculated by XRD analysis to be 11-16 nm, and the phase of the sintered alloys was observed. The fine grain size of the powders increased the austenite stability in the sintered alloys, and hence, volume fractions of metastable austenite higher than 64% existed at room temperature. The stability of austenite increased with increased carbon content. The behavior of strain-induced martensite transformation during deformation was evaluated using the BMT model, and the variation of austenite stability at different carbon contents was evaluated by comparing the *k* values.

Acknowledgments

This research was supported by Basic Science Research Program through the National Research Foundation of Korea (NRF) funded by the Ministry of Education (2016R1D1A1B03935163).

REFERENCES

[1] S. Lee, S.J. Lee, S.S. Kumar, K. Lee, B.C. De Cooman, Metall. Mater. Trans. A. **42A**, 3638 (2011).
[2] J.M. Torralba, A. Navarro, M. Campos, Mater. Sci. Eng. A. **573**, 253 (2013).
[3] G. Frommeyer, U. Brux, P. Neumann, ISIJ Int. **43**, 438 (2003).
[4] Y. Sakuma, O. Matsumura, H. Takechi, Metall. Trans. A. **22A**, 489 (1991).
[5] G.N. Haidemenopoulos, A.T. Kermanidis, C. Malliaros, H.H. Dickert, P. Kucharzyk, W. Bleck, Mater. Sci. Eng. A. **573**, 7 (2013).
[6] S.J. Lee, S. Lee, B.C. De Cooman, Int. J. Mater. Res. **104**, 423 (2013).
[7] Y. Matsuoka, T. Iwasaki, N. Nakada, T. Tsuchiyama, S. Takaki, ISIJ Int. **53**, 1224 (2013).
[8] C. Suryanarayana, Prog. Mater Sci. **46**, 1 (2001).
[9] C. Keller, K. Tabalaiev, G. Marnier, J. Noudem, X. Sauvage, E. Hug, Mater. Sci. Eng. A. **665**, 125 (2016).
[10] W. Ju, Y.D. Kim, J.J. Sim, S.H. Choi, S.K. Hyun, K.M. Lim, K.T. Park, J. Korean Powder Metall. **24**, 377 (2018).
[11] S.J. Oh, D. Park, K. Kim, I.J. Shon, S.J. Lee, Mater. Sci. Eng. A. **725**, 382 (2018).
[12] S.J. Oh, I.J. Shon, S.J. Lee, J. Korean Powder Metall. **25**, 126 (2018).
[13] V.X.L. Filho, I.F. Barros, H.F.G. Abreu, Mater. Res. **20**, 10 (2017).
[14] Y. Ustinovshikov, I. Shabanova, J. Alloys Compd. **578**, 292 (2013).
[15] M.B. Shongwe, M.M. Ramakokovhu, S. Diouf, M.O. Durowoju, B.A. Obadele, R. Sule, M.L. Lethabane, P.A. Olubambi, J. Alloys Compd. **678**, 241 (2016).
[16] K.B. Reuter, D.B. Williams, J.I. Goldstein, Metall. Trans. A **20**, 719 (1989)
[17] C. Kuhrt, L. Schultz, J. Appl. Phys. **73**, 1975 (1993).
[18] G.K. Williamson, W.H. Hall, Acta Metall. **1**, 22 (1953).
[19] I. Mobasherpour, A.A. Tofigh, M. Ebrahimi, Mater. Chem. Phys. **138**, 535 (2013).
[20] B.L. Averbach, M. Cohen, Trans. AIME. **196**, 1 (1948).
[21] K. Kim, S.J. Oh, D. Park, I.J. Shon, S.J. Lee, Mater. Trans. **59**, 1206 (2018).
[22] H. Shirazi, G. Miyamoto, S.H. Nedjad, T. Chiba, M.N. Ahmadabadi, T. Furuhara, Acta Metall. **144**, 269 (2018).
[23] D. Park, S.J. Oh, I.J. Shon, S.J. Lee, Arch. Metall. Mater. **63**, 1479 (2018).
[24] S. Lee, S.J. Lee, B.C. De Cooman, Scr. Mater. **65**, 225 (2011).
[25] C.Y. Wang, Y. Chang, X.D. Li, K.M. Zhao, H. Dong, Sci. CHINA Technol. Sc. **59**, 832 (2016).
[26] J. Burke, Kinetics of Phase Transformation in Metals, Pergamon Press, Oxford, United Kingdom, 1965.
[27] O. Matsumura, Y. Sakuma, H. Takechi, Scr. Mater. **21**, 1301 (1987).
[28] N. Tsuchida, Y. Tomota, Mater. Sci. Eng. A **285**, 345 (2000).